EARTHQUAKE ENGINEERING AND STRUCTURAL DYNAMICS
Earthquake Engng Struct. Dyn. 2003; **32**:2267–2288 (DOI: 10.1002/eqe.331)

Evaluation of predictors of non-linear seismic demands using 'fishbone' models of SMRF buildings

Nicolas Luco[1,*,†], Yasuhiro Mori[2], Yosuke Funahashi[3], C. Allin Cornell[1] and Masayoshi Nakashima[4]

[1]*Department of Civil and Environmental Engineering, Stanford University, Stanford, CA 94305-4020, U.S.A*
[2]*Division of Environmental Engineering and Architecture, Nagoya University, Nagoya 464-8603, Japan*
[3]*Department of Architecture, Nagoya University, Nagoya 464-8603, Japan*
[4]*Disaster Prevention Research Institute, Kyoto University, Gokasho, Uji, Kyoto 611-0011, Japan*

SUMMARY

Predictors (or estimates) of seismic structural demands that are less computationally time-consuming than non-linear dynamic analysis can be useful for structural performance assessment and for design. In this paper, we evaluate the bias and precision of predictors that make use of, at most, (i) elastic modal vibration properties of the given structure, (ii) the results of a non-linear static pushover analysis of the structure, and (iii) elastic and inelastic single-degree-of-freedom time-history analyses for the specified ground motion record. The main predictor of interest is an extension of first-mode elastic spectral acceleration that additionally takes into account both the second-mode contribution to (elastic) structural response and the effects of inelasticity. This predictor is evaluated with respect to non-linear dynamic analysis results for 'fishbone' models of steel moment-resisting frame (SMRF) buildings. The relatively small number of degrees of freedom for each fishbone model allows us to consider several short-to-long period buildings and numerous near- and far-field earthquake ground motions of interest in both Japan and the U.S. Before doing so, though, we verify that estimates of the bias and precision of the predictor obtained using fishbone models are effectively equivalent to those based on typical 'full-frame' models of the same buildings. Copyright © 2003 John Wiley & Sons, Ltd.

KEY WORDS: seismic drift demands; steel moment-resisting frame buildings; fishbone models; inelastic time-history analysis; near-field earthquake ground motions; non-linear dynamic analysis

1. MOTIVATION

In this paper we investigate 'predictors' of seismic structural demands (e.g., interstory drift) that are less time-consuming and more convenient to compute than the results of non-linear

* Correspondence to: Nicolas Luco, P.O. Box 9216, Berkeley, CA 94709, U.S.A.
† E-mail: nico.luco@stanfordalumni.org

Contract/grant sponsor: NSF (National Science Foundation); contract/grant number: CMS-9821096
Contract/grant sponsor: Ministry of Education, Science, Sports, & Culture and Japan Society for the Promotion of Science; contract/grant number: 11209204

Received 24 October 2002
Revised 7 April 2003
Accepted 7 April 2003

dynamic analysis (NDA). Specifically, the predictors that we investigate make use of (i) elastic modal vibration properties of the given structure, (ii) results of a non-linear static pushover (NSP) analysis of the structure, and (iii) elastic and inelastic spectral displacements for the ground motion. Such information is commonly available for a given structure and a specified ground motion. Under these constraints, we search for unbiased and 'precise' predictors of the non-linear structural demands. As explained in more detail in Section 7, the bias of a predictor is defined as the average ratio of the 'true' seismic structural demand (e.g., from NDA) to the value of its predictor. The precision of a predictor is measured by the variability of the 'true' structural demands *given* (i.e., conditioned on knowing) the value of the predictor.

Our primary use of predictors is structural performance assessment—that is, to estimate (i) the structural demand induced by a particular ground motion, (ii) the structural demand statistics for a suite of representative ground motions, or, more ambitiously, (iii) the mean annual frequency of exceeding a particular seismic demand (called the 'demand hazard') for a given structure at a designated site. In all of these cases, an unbiased and precise predictor, or a precise predictor for which the bias is known, can be used in lieu of NDA to estimate demand. In the case of the demand hazard for a specific structure, the use of a simulation-based approach, for example, requires structural demand estimates for 100s (or 1000s) of earthquake records [1], so the computational savings and increased viability associated with using a predictor (instead of NDA) can be particularly significant. Even if a predictor is biased, as long as it is precise one can estimate its bias with relatively few NDAs (as demonstrated briefly in Section 8.1), or one can assume a value for the bias based on generic results like those presented in this paper. Furthermore, the variability of 'true' structural demands given the value of a predictor (i.e., the precision) can be accounted for by (i) adopting a higher fractile value (such as the 'mean plus one sigma'), (ii) appropriately inflated load factors, e.g., Reference [2], or (iii) an integrated structural demand hazard determination, via Probabilistic Seismic Demand Analysis [3, 4], for example.

The predictors investigated in the paper can also be used in structural design. During preliminary or conceptual design, when detailed member-by-member properties are not available and therefore NDA cannot be carried out, a predictor can be roughly calculated as an estimate of the non-linear seismic demands—refer to Section 6 for an example. Predictors can be used in lieu of NDA to evaluate subsequent design iterations, as well. Even though NDA is widely accepted to be the most accurate analysis procedure, it is seldom, if ever, performed in the design of low- to mid-rise buildings, for example. In these cases, simpler methods of estimating seismic demands, such as the predictors investigated in the paper, can be especially useful.

2. OBJECTIVES

In this paper we evaluate, with respect to the results of NDA (non-linear dynamic analysis), the bias and precision of two different predictors of seismic interstory drift demands. Specifically, the interstory drift demands considered are peak (over time) story drift angle, denoted θ_i for story i, and maximum (over all stories) peak story drift angle, denoted $\theta_{\max}$; the two are referred to generically as θ. We consider both U.S. and Japanese low- to high-rise SMRF (steel moment-resisting frame) buildings of short (0.2 sec) to long (4 sec) fundamental period, as well as near- and far-field earthquake ground motions recorded in both the U.S. and Japan.

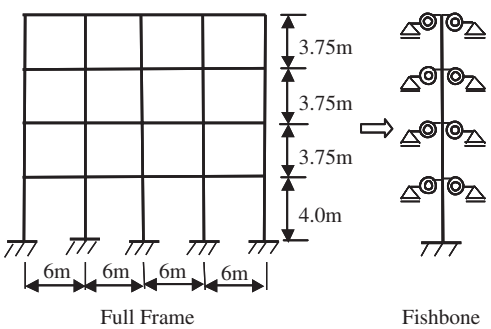

Figure 1. Schematic representations of (a) the full-frame and (b) the fishbone models of the JP4 building.

Since NDA of even the two-dimensional building models considered in this paper can be rather computationally intensive, a 'fishbone,' or 'generic frame' model [5, 6] of each building is analyzed to compute the 'true' seismic demands. The computational savings associated with fishbone models (such as the one illustrated in Figure 1(b)) allow us to consider a large number of ground motions. Before focusing solely on fishbone models, however, we first verify that the evaluation of predictors using fishbone versus 'full-frame' models yields comparable estimates of bias and precision.

3. PREDICTORS

The two predictors of seismic non-linear structural drift demands that are investigated in this paper, denoted $\hat{\theta}^{1E}$ and $\hat{\theta}^{1I\&2E}$, have formerly been examined from the perspective of ground motion intensity measures (denoted IM_{1E} and $IM_{1I\&2E}$) in References [7, 8]. Nevertheless, here we provide sufficient information for the reader to calculate both predictors, and in Section 6 we provide a detailed example of such calculations. Here we also comment on 'intermediate' versions of the predictors $\hat{\theta}^{1E}$ and $\hat{\theta}^{1I\&2E}$ that are not explicitly considered in this paper, but are considered in References [7, 8].

3.1. First-mode-elastic predictor

Although more commonly thought of as a ground motion intensity measure, the fundamental-mode spectral displacement $S_d(T_1, \zeta_1)$ (where T_1 and ζ_1 are the first-mode period and damping ratio, respectively) can also be considered as a predictor if multiplied by a modal participation factor for θ. Such predictors of θ_i and θ_{max}, denoted here as $\hat{\theta}_i^{1E}$ and $\hat{\theta}_{max}^{1E}$, are expressed in Equation (1), where n is the total number of stories (or floors) in the given building model. Note that in modal analysis, $\hat{\theta}^{1E}$ is simply the first-mode elastic estimate of θ.

$$\hat{\theta}_i^{1E} = PF_1^{\theta_i} S_d(T_1, \zeta_1) \tag{1a}$$

$$\hat{\theta}_{max}^{1E} = \max_{i=1:n}(\hat{\theta}_i^{1E}) \tag{1b}$$

The participation factor $PF_1^{\theta_i}$ is defined generally in Equation (2), where $\phi_{j,i}$ is the element of the j-th modal vector that corresponds to the upper floor of the i-th story (i.e., the i-th floor, with $\phi_{j,0}=0$), h_i is the height above ground of the i-th floor (in the same units used for spectral displacement, with $h_0=0$), and m_i is the mass of the i-th floor. Note that Γ_j is also commonly referred to as a participation factor, e.g., Reference [9].

$$PF_j^{\theta_i}=\Gamma_j\frac{\phi_{j,i}-\phi_{j,i-1}}{h_i-h_{i-1}} \quad \text{where} \quad \Gamma_j=\frac{\sum_{i=1:n}\phi_{j,i}m_i}{\sum_{i=1:n}\phi_{j,i}^2 m_i} \tag{2}$$

Consistent with the criteria stated in Section 1, the predictor $\hat{\theta}^{1E}$ only requires modal vibration properties of the given structure (i.e., T_1, ζ_1, and $PF_1^{\theta_i}$) and an elastic single-degree-of-freedom (SDOF) time-history analysis to compute $S_{\mathrm{d}}(T_1,\zeta_1)$. In this paper, $\hat{\theta}^{1E}$ is used as a basis of comparison for the main predictor of interest, described next.

3.2. First-mode-inelastic and second-mode-elastic predictor

The main predictor investigated in this paper is denoted $\hat{\theta}^{1I\&2E}$. As an extension of $\hat{\theta}^{1E}$, $\hat{\theta}^{1I\&2E}$ makes use of elastic modal vibration properties, a NSP (non-linear static pushover) curve, and elastic and inelastic SDOF time-history analyses. As expressed in Equation (3), $\hat{\theta}^{1I\&2E}$ is the product of (i) the ratio of a first-mode inelastic spectral displacement, $S_{\mathrm{d}}^I(T_1,\zeta_1,d_y,\alpha)$, to the first-mode elastic spectral displacement, $S_{\mathrm{d}}(T_1,\zeta_1)$, and (ii) the elastic estimate of θ computed using the first two modes and the square-root-of-sum-of-squares (SRSS) rule of modal combination. Note that the elastic third mode can be (and is, in Section 8.3) easily added to $\hat{\theta}^{1I\&2E}$.

$$\hat{\theta}_i^{1I\&2E}=\frac{S_{\mathrm{d}}^I(T_1,\zeta_1,d_y,\alpha)}{S_{\mathrm{d}}(T_1,\zeta_1)}\sqrt{[PF_1^{\theta_i}S_{\mathrm{d}}(T_1,\zeta_1)]^2+[PF_2^{\theta_i}S_{\mathrm{d}}(T_2,\zeta_2)]^2} \tag{3a}$$

$$\hat{\theta}_{\max}^{1I\&2E}=\max_{i=1:n}(\hat{\theta}_i^{1I\&2E}) \tag{3b}$$

Recall that the elastic participation factors $PF_1^{\theta_i}$ and $PF_2^{\theta_i}$ were defined above in Equation (2). The use of 'inelastic participation factors' (e.g., based on story-drift results from a NSP analysis) is mentioned at the conclusion of this paper (Section 10).

Note that the bilinear inelastic spectral displacement $S_{\mathrm{d}}^I(T_1,\zeta_1,d_y,\alpha)$ is parameterized by the yield displacement d_y and strain hardening ratio α, in addition to T_1 and ζ_1. In this paper, the parameters d_y and α are determined from a NSP curve (base shear versus roof drift angle) for the given building model. As detailed in Appendix A, an elastic–perfectly-plastic backbone curve (i.e., $\alpha=0$) is fit to the NSP curve, except when the NSP curve exhibits significant strain hardening and does not degrade; in this latter case, a bilinear backbone curve is fit. A trilinear idealization of the NSP curve is also an option, as mentioned is Section 9.4.

3.3. Intermediate predictors

Two other predictors intermediate to $\hat{\theta}^{1E}$ and $\hat{\theta}^{1I\&2E}$, namely a 'first-mode-inelastic' and a 'first-and-second-mode-elastic' predictor (which could be denoted as $\hat{\theta}^{1I}$ and $\hat{\theta}^{1E\&2E}$, respectively)

have been investigated (as ground motion intensity measures) in References [7, 8], but are not explicitly considered in this paper. Note, however, that for structures for which the contribution of higher modes to the (elastic) response is negligible (e.g., short-period, low-rise buildings), the predictor $\hat{\theta}^{1I\&2E}$ is practically equivalent to $\hat{\theta}^{1I}$. For longer-period structures (e.g., high-rise buildings), on the other hand, $\hat{\theta}^{1I\&2E}$ is roughly equivalent to $\hat{\theta}^{1E\&2E}$ (at least for non-near-field earthquake records) as a consequence of the 'equal displacements rule' [10]. For mid-rise buildings, though, $\hat{\theta}^{1I\&2E}$ differs from $\hat{\theta}^{1I}$ and $\hat{\theta}^{1E\&2E}$, and in References [7, 8] it is found to be less biased and more precise than the two intermediate predictors.

4. BUILDING MODELS

In order to evaluate the two predictors described in the previous section, two-dimensional fishbone and full-frame models of a low-, a mid-, and a high-rise SMRF building are considered; the four-, nine-, and twenty-story buildings are denoted as JP4, SAC9, and SAC20, respectively. In addition, in order to evaluate the predictors for a very short-period structure, a fishbone model of SAC9 with artificially increased modulus of elasticity (by a factor of 100) is also considered; this artificial structure is denoted as SAC9S. The first- and second-mode periods and damping ratios of each building model are listed in Table I. For simplicity, a second-mode damping ratio of 2% is always assumed in calculating $\hat{\theta}^{1I\&2E}$. Other details specific to each of the three buildings are provided in the subsections below, including NSP curves for both the fishbone and full-frame models. The values of d_y and α for the predictor $\hat{\theta}^{1I\&2E}$, which are based on these NSP curves (as described in Appendix A), are also listed in Table I.

As illustrated in Figure 1 (for the JP4 building), the fishbone model of a frame condenses all of the columns in a story into a single column, and all of the beams in a floor into a single rotational beam spring, thereby significantly reducing the number of degrees of freedom. The key assumption is that the rotations at all of the beam–column connections in a floor are identical. The details of this condensation are explained in References [5, 6], but

Table I. First- and second-mode periods and modal damping ratios for the fishbone and full-frame models considered in this paper, as well as yield displacements (d_y) and strain hardening ratios (α) estimated from their non-linear static pushover curves (i.e., Figures 2 and A1).

Building model		T_1 (sec)	T_2 (sec)	ζ_1 (%)	ζ_2 (%)	d_y (cm)	α (%)
SAC9	Full-frame	2.29	0.86	2.0	1.1	28	0
	Fishbone	2.24	0.84	2.0	1.1	26	0
JP4	Full-frame	0.80	0.29	2.0	2.0	10	0
	Fishbone	0.75	0.27	2.0	2.0	9.2	0
SAC20	Full-frame	3.96	1.27	2.0	1.2	39	0
	Fishbone	3.82	1.37	2.0	1.2	36	0
SAC9S	Fishbone	0.22	0.082	2.0	2.0	0.39	3

a few important characteristics of the fishbone models considered in this paper are listed here:

(i) The single beam spring for each floor is trilinear, with a strain-hardening (i.e., third) slope equal to 2% (3% for SAC9) of the elastic slope. The elastic (i.e., initial) stiffness of each beam spring takes into account the effect of axial deformations in the outer columns of the frame caused by overturning.
(ii) Bilinear plastic hinging at the column ends (of each story) and at splices is modeled, with 3% (1% for JP4) strain hardening. Column P–M interactions due to tributary gravity loads, but not due to varying axial forces caused by overturning, are taken into account.
(iii) Global (but not member) P–Δ effects are accounted for, with all applicable gravity loads placed on the fishbone column (or columns, as described below for the SAC20 building).

The corresponding 'full-frame' models of the buildings, on the other hand, are simple member-by-member centerline models that account for beam plastic-hinging (concentrated plasticity) with 2% strain hardening (3% for SAC9), plastic hinging at column ends and splices with 3% strain hardening (1% for JP4), P–M interaction, and global (but not member) P–Δ effects. All of the building models, whether full-frame or fishbone, are analyzed using DRAIN-2DX [11].

4.1. SAC9 building

SAC9 is a 9-story perimeter SMRF building designed for Los Angeles conditions by consulting structural engineers as part of Phase II of the SAC Steel Project [12]. In both the fishbone and full-frame models of the SAC9 building, only one of the 5-bay perimeter MRFs is modeled, but gravity loads from half of the building are considered since they contribute to the effects of P–Δ. The interior frames are assumed to resist gravity loads only. This full-frame model of SAC9 is the same 'M1' model commonly considered by SAC investigators, e.g., References [7, 12], with one difference—here the basement is ignored and the columns are assumed to be fixed at the ground level. The NSP curves for the fishbone and full-frame models of SAC9 are shown in Figure 2. Note the significant effect of P–Δ, particularly beyond a roof drift angle of about 0.05 rad. A NSP curve for the artificial SAC9S fishbone model is provided in Appendix A.

4.2. JP4 building

JP4 is a 4-story SMRF building designed by a structural engineer according to Japanese practices [13]. Unlike SAC9 (or SAC20 to follow), all of the perimeter and interior frames, and all of the beam–column connections of JP4 are moment resisting. Only one of these frames is modeled, taking into account its tributary gravity loads—an elevation view of the 4-bay MRF considered is shown in Figure 1(a). The NSP curves for the fishbone and full-frame models of JP4 are shown in Figure 2. Note that the effect of P–Δ is negligible because JP4 is relatively stiff and only the tributary gravity loads contribute to P–Δ, as opposed to gravity loads from one-half of the building like for the SAC9 (and SAC20) perimeter MRF.

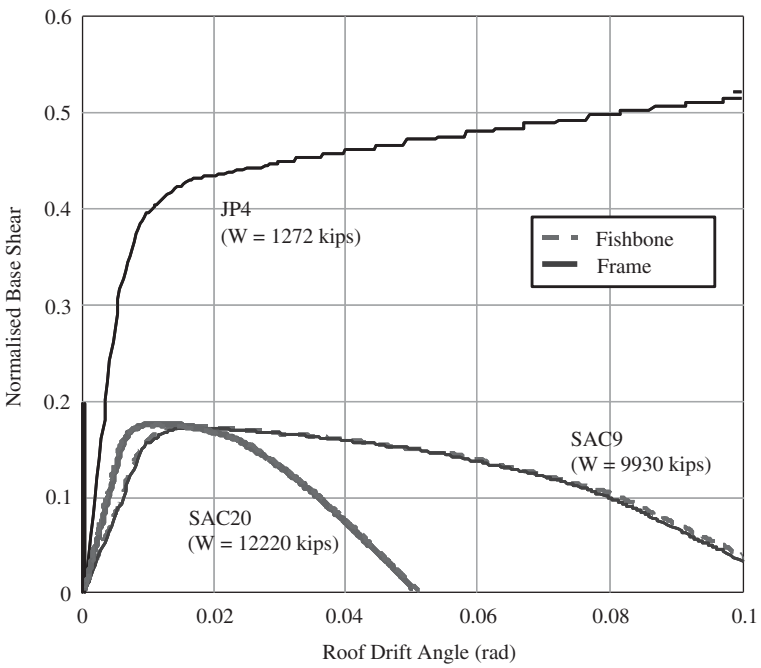

Figure 2. Non-linear static pushover curves for the fishbone and full-frame models of the SAC9, JP4, and SAC20 buildings.

4.3. SAC20 building

SAC20 is a 20-story perimeter SMRF building that, like SAC9, was designed for Los Angeles conditions as part of the SAC Steel Project (Phase II). Unlike SAC9, both a 5-bay perimeter MRF and a 3-bay interior gravity frame of SAC20 (as well as columns that are part of the orthogonal perimeter MRFs) are modeled. For both the fishbone and full-frame models, separate representations of the perimeter and interior frames (and the additional columns) are linked together at each floor under the assumption of a rigid diaphragm. Furthermore, rather than modeling the shear connections (e.g., in the interior gravity frames) as 'pins', each of them is attributed stiffness and strength properties reasonably close to those observed in laboratory tests [14]. Note that the full-frame model considered here is the same one considered in Reference [8] and detailed in Reference [7]. The NSP curves for the fishbone and full-frame models of SAC20 are shown in Figure 2. Note the very significant effect of P–Δ, even at roof drift angles as small as 0.02 rad.

5. EARTHQUAKE GROUND MOTION RECORDS

In conjunction with the building models described in the previous section, the earthquake record sets detailed here are used to evaluate the bias and precision of each of the predictors.

The sets include ground motions recorded at both near- and far-field sites in the U.S. and Japan. Note that a relatively large number of earthquake records are considered here; nonlinear dynamic analyses for this many earthquake records is not overly time-consuming when fishbone models are used.

5.1. Nearby-field set

The so-called 'nearby-field' earthquake records were selected from the PEER Strong Motion Database (http://peer.berkeley.edu/smcat) according to the following criteria: (i) closest distance to the rupture surface, R_{close}, less than 16 km, (ii) earthquake moment magnitude, M_w, greater than or equal to 6.0, (iii) recorded on 'stiff soil' or 'very dense soil and soft rock' (e.g., FEMA 273 site classes D or C, respectively), and (iv) high-pass-filter corner frequency less than or equal to 0.25 Hertz. Only the strike-normal components are used. Of the resulting 75 nearby-field ground motions, 72 were recorded in California, and the other 3 were recorded in Erzican (Turkey), Tabas (Iran), and Kobe—refer to Reference [7] for a detailed list. Note that this set of earthquake records (and the far-field set to follow) was collected before the 1999 earthquakes in Taiwan and Turkey.

Despite their proximity to the earthquake source, it is important to note that not all of the nearby-field earthquake records are 'pulse-like' (i.e., not all exhibit a low-frequency, large-amplitude pulse in the velocity time history). In fact, less than half of the nearby-field ground motions are recorded in the region where forward rupture-directivity effects are anticipated, and even those are not all pulse-like [7]. As detailed below, a set of pulse-like earthquake records is considered separately.

5.2. Far-field set

The far-field earthquake records were also selected from the PEER Strong Motion Database (http://peer.berkeley.edu/smcat) according to the same criteria used for the nearby-field set, except that R_{close} is limited to greater than or equal to 30 km and less than 46 km. As for the nearby-field set, only the strike-normal components are used, and recordings from the 1999 earthquakes in Taiwan and Turkey are not included. Of the resulting 75 earthquake records, 74 were recorded in California and one was recorded in Kobe—refer to Reference [7] for a detailed list.

5.3. Kobe set

The Kobe set consists of the 11 ground motions recorded within 8.7 km of the fault surface that ruptured during the Kobe earthquake of 1995 ($M_w = 6.9$)—refer to Reference [15] for a list of the station names. Like the nearby- and far-field earthquake records, only the strike-normal components are considered. As R_{close} is less than 16 km for all of these Kobe earthquake records, they could also be classified as 'nearby'; like the nearby-field earthquake records, though, the Kobe earthquake records are not necessarily 'pulse-like'. Note that only one of the Kobe earthquake records (KJMA) is also part of the nearby-field set because the other 10 were not recorded on 'stiff soil' or 'very dense and soft rock'.

5.4. Pulse-like set

The pulse-like set consists of the 14 strike-normal earthquake records deemed by Alavi and Krawinkler [16] to exhibit a low-frequency, large amplitude pulse. Eight of these earthquake records are also part of the nearby-field set. The other six earthquake records would be included in the nearby-field set if not for the fact that they were not originally recorded on 'stiff soil' or 'very dense soil and soft rock'; Somerville *et al.* [17, 18] did, however, modify these records to reflect stiff soil conditions. Refer to Reference [7] for details of the pulse-like earthquake records.

6. NUMERICAL EXAMPLE OF CALCULATING PREDICTORS

To demonstrate the straightforward calculation of the two predictors investigated in this paper, here we provide the details of a numerical example in which both predictors are calculated for one of the nearby-field earthquake records and the full-frame model of the JP4 building. The specific earthquake record considered is the Sylmar Olive View (SYL) recording of the 1994 Northridge earthquake.

6.1. First-mode-elastic predictor, $\hat{\theta}^{1E}$

As expressed in Equation (1), the first component of the predictor $\hat{\theta}_i^{1E}$ is the building's first-mode participation factor, $PF_1^{\theta_i}$, which is calculated according to Equation (2) as a function of the floor heights (h_i), the floor masses (m_i), and the first modal vector ($\phi_{1,i}$). For the full-frame model of the JP4 building, $h_i = \langle 400, 775, 1150, 1525 \rangle$ cm, $m_i = \langle 1.44, 1.44, 1.44, 1.44 \rangle \times 10^5$ kg/(cm/s^2), and, from a simple eigenvector analysis, $\phi_{1,i} = \langle 0.27, 0.55, 0.79, 1.00 \rangle$ (dimensionless). Note that, in general, $\phi_{1,i}$ can easily be approximated by assuming a linear mode shape. Plugging h_i, m_i, and $\phi_{1,i}$ into Equation (2) yields $PF_1^{\theta_i} = \langle 8.67, 9.77, 8.55, 7.20 \rangle \times 10^{-4}$ cm^{-1}.

The second component of the predictor $\hat{\theta}_i^{1E}$ is the first-mode elastic spectral displacement for the ground motion, $S_d(T_1, \zeta_1)$. For the full-frame model of the JP4 building, recall from Table I that the first-mode period and damping ratio are $T_1 = 0.80$ s and $\zeta_1 = 2\%$. Here T_1 is the result of a simple eigenvalue analysis, but it could instead be estimated via a simple code equation, e.g., Reference [19]; as is typical, ζ_1 is assumed for the given type of structural system. Computed via a single elastic time-history analysis for the Sylmar earthquake record, or simply read from its response spectrum, $S_d(T_1, \zeta_1) = 43.3$ cm.

Finally, multiplying $PF_1^{\theta_i}$ and $S_d(T_1, \zeta_1)$ gives $\hat{\theta}_i^{1E} = \langle 0.038, 0.042, 0.037, 0.031 \rangle$ rad, and the maximum of these values is $\hat{\theta}_{\max}^{1E} = 0.042$ rad. From a non-linear dynamic analysis of the full-frame model of JP4 subjected to the Sylmar earthquake record, $\theta_{\max} = 0.029$ rad. Hence, in this example $\hat{\theta}_{\max}^{1E}$ over-predicts $\theta_{\max}$ by a factor of almost 1.5. Note, however, that based on the average of all 75 of the nearby-field earthquake records, $\hat{\theta}_{\max}^{1E}$ is found in Section 9.3 to be unbiased for the fishbone model of JP4.

6.2. First-mode-inelastic and second-mode-elastic predictor, $\hat{\theta}^{1I\&2E}$

As expressed in Equation (3), the first component of the predictor $\hat{\theta}_i^{1I\&2E}$ is the ratio of the first-mode inelastic to elastic spectral displacements for the ground motion, $S_d^I(T_1, \zeta_1, d_y, \alpha)$/

$S_d(T_1, \zeta_1)$. Recall that the yield displacement d_y and strain-hardening ratio α are estimated from a NSP (non-linear static pushover) curve for the building model, as detailed in Appendix A. For the full-frame model of the JP4 building, α is set equal to 0% and d_y is estimated from its NSP curve (in Figure 2) to be 10.1 cm. More specifically, the roof drift angle at yield, denoted $(\theta_{\text{roof}})_y$, is estimated to be 0.0086 rad, and hence $d_y = (\theta_{\text{roof}})_y / PF_1^{\theta_{\text{roof}}} = 0.0086/8.55 \times 10^{-4} =$ 10.1 cm according to Equation (A2) of Appendix A. Computed via a single SDOF inelastic time-history analysis for the Sylmar earthquake record, $S_d^I(T_1, \zeta_1, d_y, \alpha) = 26.6$ cm, and from the calculation of $\hat{\theta}^{1E}$ in the previous subsection, $S_d(T_1, \zeta_1) = 43.3$ cm; hence, $S_d^I(T_1, \zeta_1, d_y, \alpha)/S_d(T_1, \zeta_1) = 0.61$. Note that this is a case in which the inelastic spectral displacement is less than its elastic counterpart.

The second component of the predictor $\hat{\theta}_i^{1I\&2E}$ is the first-two-mode elastic SRSS estimate of each story drift angle (i.e., the square root term in Equation (3)). For the first-mode-dominated full-frame model of the JP4 building, this component is approximately equal (to two significant figures) to $\hat{\theta}_i^{1E} = \langle 0.038, 0.042, 0.037, 0.031 \rangle$ rad from the previous subsection; albeit unnecessary in this case, the second-mode portion can be calculated in the same manner as $\hat{\theta}_i^{1E}$. Recall from Table I that $T_2 = 0.29$ s and $\zeta_2 = 2\%$, and note that $\phi_{2,i} = \langle -0.76, -1.00, -0.32, 1.00 \rangle$. The second-mode elastic spectral displacement for the Sylmar earthquake record is $S_d(T_2, \zeta_2) =$ 2.00 cm.

Finally, multiplying the ratio $S_d^I(T_1, \zeta_1, d_y, \alpha)/S_d(T_1, \zeta_1)$ by the first-two-mode elastic SRSS term gives $\hat{\theta}_i^{1I\&2E} = \langle 0.023, 0.026, 0.023, 0.019 \rangle$ rad, and the maximum of these values is $\hat{\theta}_{\max}^{1I\&2E} = 0.026$rad. Recall from the previous subsection that from a non-linear dynamic analysis of the full-frame model of JP4 subjected to the Sylmar earthquake record, $\theta_{\max} = 0.029$ rad. Hence, in this example the ratio of $\theta_{\max}$ to $\hat{\theta}_{\max}^{1I\&2E}$ is 1.11, which (by design) happens to be approximately equal to the bias of $\hat{\theta}_{\max}^{1I\&2E}$ for the full-frame model of JP4 determined in Section 8.3 from the results of all 75 nearby-field earthquake records.

7. METHOD FOR EVALUATING PREDICTORS

Before evaluating the predictors for all of the building models and earthquake records considered in this paper, here we specify precisely how we establish the bias and precision of a predictor. The bias of a predictor, denoted here simply as a, is calculated as the 'median' of $\theta/\hat{\theta}$—that is, the ratio of (i) the demand computed via non-linear dynamic analysis of the model structure, to (ii) the corresponding value of the predictor. Here the median refers to the exponential of the average of the natural logarithms of $\theta/\hat{\theta}$ (i.e., the geometric mean). The precision of a predictor is measured by the 'dispersion' of $\theta/\hat{\theta}$, denoted here simply as σ; the dispersion refers to the standard deviation of the natural logarithms of $\theta/\hat{\theta}$. Since σ is also the dispersion of $\hat{\theta}$ given θ, it gives the width of a confidence interval for θ centered around $a \cdot \hat{\theta}$. The smaller σ is, the narrower the confidence interval for θ, and the more precise is $\hat{\theta}$.

Instead of calculating the bias a and precision σ as the median and dispersion of $\theta/\hat{\theta}$, a and σ can equivalently be obtained by performing a one-parameter log–log linear least squares regression of θ on $\hat{\theta}$. The regression model is expressed in Equation (4), where a is the regression parameter and ε is the random error in θ given $\hat{\theta}$ with (by definition) median 1

and dispersion σ.

$$\ln(\theta) = \ln(a) + \ln(\hat{\theta}) + \ln(\varepsilon) \tag{4}$$

A fundamental assumption of this, and any standard linear regression analysis, is that ε is independent of $\hat{\theta}$ (i.e., homoskedasticity). For a number of the regression results to follow, however, we see from plots of θ versus $\hat{\theta}$ that this assumption does not strictly hold. In some of these cases, a two-parameter regression model that includes a second coefficient on the $\ln(\hat{\theta})$ term in Equation (4) could instead be employed to ensure homoskedasticity. In a two-parameter model, however, the coefficient a cannot be interpreted as the bias of the predictor $\hat{\theta}$ in estimating the demand θ, and the precision of the predictor is not simply equal to the dispersion about the regression fit σ. For these reasons, the one-parameter regression approach is used in the following sections to calculate the bias (a) and precision (σ) of the predictors.

8. FISHBONE VERSUS FULL-FRAME EVALUATION OF PREDICTORS

To verify that using fishbone models to evaluate the bias and precision of the predictors is effectively equivalent to using the corresponding full-frame models of the buildings, in this section both the fishbone and the full-frame model results from NDA (non-linear dynamic analysis) are used to evaluate the predictor $\hat{\theta}^{1I\&2E}$. All three of the SMRF buildings described in Section 4, and all four of the earthquake record sets described in Section 5 are considered, but not every combination. For the SAC9 models, all of the earthquake records are considered, but for the JP4 and SAC20 models, only the nearby-field set is used. In all of these cases, the predictions of $\theta_{\max}$ (the max peak story drift angle) are reported, but the predictions of θ_i (the peak story drift angle for story i) are only reported for the SAC9 models subjected to the nearby-field ground motions. Although not reported here in detail, the statistical significance of differences in the bias (a) and precision (σ) of $\hat{\theta}^{1I\&2E}$ for the fishbone versus full-frame models are formally tested via a two-sided t-test for a and a two-sided F-test for σ, e.g., Reference [20]. The differences are deemed to be significant if the probability of observing a discrepancy at least as large as that actually witnessed (i.e., the p-value) is less than 5%.

8.1. SAC9 building and nearby-field earthquake records

For the fishbone model of the SAC9 building subjected to the nearby-field earthquake records, the regression of $\theta_{\max}$ from NDA on the predictor $\hat{\theta}^{1I\&2E}_{\max}$ is illustrated in Figure 3(a). Note first that the values of $\theta_{\max}$ range from about 0.003 rad to nearly 0.05 rad; considering a yield drift angle of approximately 0.01 rad, the latter corresponds to a ductility of about 5. The resulting regression coefficient $a = 1.31$ is larger than unity, indicating that the predictor is somewhat biased low—that is, on average it underestimates $\theta_{\max}$. The dispersion about the regression fit $\sigma = 0.23$, on the other hand, is relatively small, indicating that the predictor is rather precise. In this case, one could estimate the bias of $\hat{\theta}^{1I\&2E}_{\max}$ (i.e., a) to within a standard error of about 10% using the results for only six earthquake records [20]. Although not reported here in detail, we have confirmed this assertion by randomly sampling (in groups of six) from the results for the full set of 75 nearby-field earthquake records.

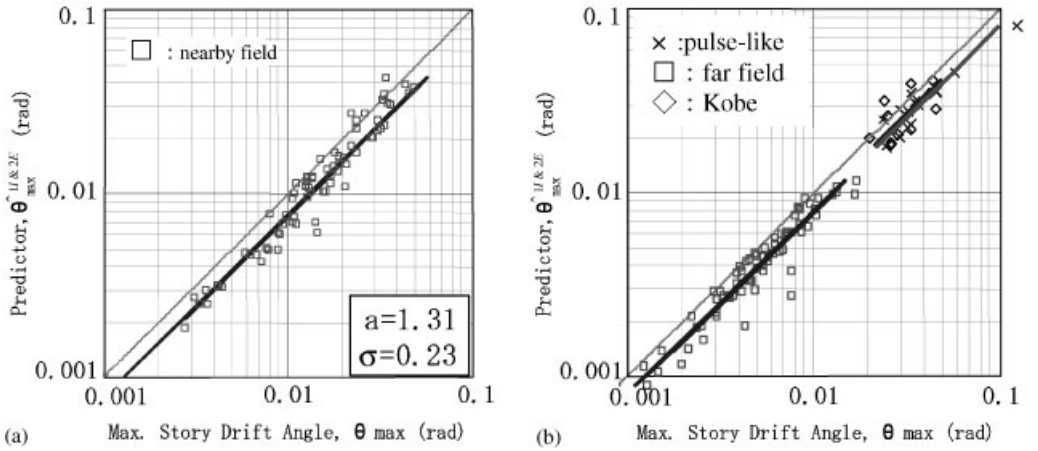

Figure 3. Regressions of $\theta_{\max}$ on $\hat{\theta}_{\max}^{1I\&2E}$ for the fishbone model of the SAC9 building subjected to (a) the nearby-field, and (b) the far-field, Kobe, and pulse-like sets of earthquake records. For the latter, the regression estimates of the bias (a) and precision (σ) of the predictor are listed in Table III.

Table II. Bias (a) and precision (σ) of the predictors $\hat{\theta}_i^{1I\&2E}$ and $\hat{\theta}_{\max}^{1I\&2E}$ for the full-frame model of the SAC9 building subjected to the nearby-field earthquake records.

Story	Bias, a	Precision, σ
1	1.02	0.20
2	1.04	0.16
3	1.10	0.15
4	1.18	0.19
5	1.15	0.23
6	1.06	0.24
7	1.05	0.22
8	1.13	0.22
9	1.23	0.28
Max	1.25	0.19

Analogous to Figure 3(a), the regression results for θ_i are illustrated in Figure 4. Note that a and σ vary amongst the different stories—this is due to, among other things, the effects of higher (than second) modes, P–Δ effects, and the 'isolation' of upper stories resulting from yielding in lower stories. The values of a range from 1.03 in the 1st story to 1.29 in the 9th story, and the values of σ range from 0.17 in the 3rd story to 0.36 in the 9th story.

For the corresponding full-frame model of SAC9, the regression results to be compared with Figures 3(a) and 4 are listed in Table II. Note first that the bias and precision of $\hat{\theta}_{\max}^{1I\&2E}$, $a = 1.25$ and $\sigma = 0.19$, are nearly the same as those found using the fishbone results (i.e., $a = 1.31$ and $\sigma = 0.23$). Neither of these differences is statistically significant in light of the approximately 20% dispersion of $\theta_{\max}$ given $\hat{\theta}_{\max}^{1I\&2E}$ (i.e., $\sigma \approx 0.2$). By comparing the

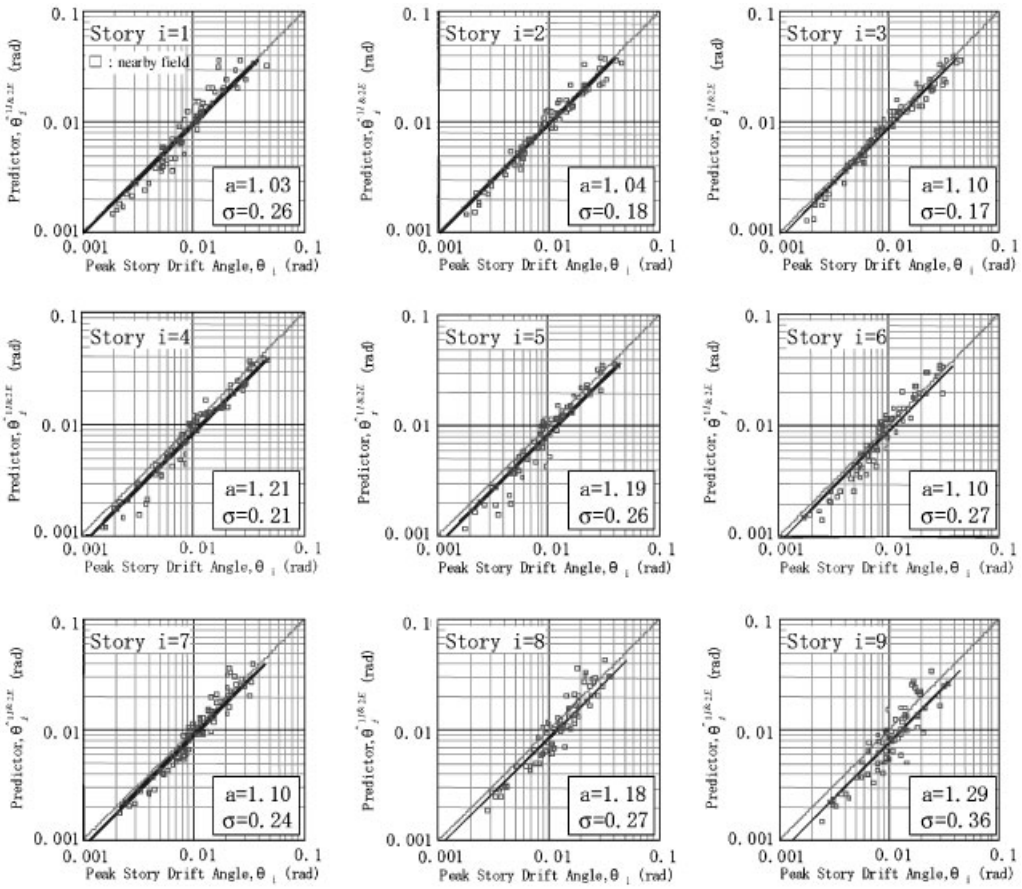

Figure 4. Regressions of θ_i on $\hat{\theta}_i^{1I\&2E}$ for the fishbone model of the SAC9 building subjected to the nearby-field earthquake records. Note the regression estimates of the bias (a) and precision (σ) of the predictor.

story-by-story results obtained using the full-frame versus fishbone models, we also find that the two estimates of the bias of $\hat{\theta}_i^{1I\&2E}$ are nearly the same at all of the stories. The two estimates of the precision of $\hat{\theta}_i^{1I\&2E}$ are about the same at all but the top and bottom stories, where the estimates of σ obtained using the fishbone results are slightly larger (i.e., $\sigma = 0.26$ vs. 0.20 for the 1st story, and $\sigma = 0.36$ vs. 0.28 for the 9th story).

8.2. SAC9 building and far-field, Kobe, and pulse-like earthquake records

Also for the SAC9 building, but subjected to the far-field, Kobe, and pulse-like sets of earthquake records, the evaluation of the bias and precision of $\hat{\theta}_{\max}^{1I\&2E}$ using the fishbone model results is illustrated in Figure 3(b). Note that $\theta_{\max}$ ranges from about 0.001 to 0.02 rad for the

Table III. Bias (a) and precision (σ) of the predictor $\hat{\theta}_{\max}^{1I\&2E}$ for the full-frame and fishbone models, and of $\hat{\theta}_{\max}^{1E}$ for the fishbone model of the SAC9 building subjected to the far-field, Kobe, and pulse-like earthquake records. The regressions performed to estimate a and σ for the fishbone models are illustrated in Figures 3(b) and 5(b).

Earthquake records	Bias, a			Precision, σ		
	$\hat{\theta}_{\max}^{1I\&2E}$		$\hat{\theta}_{\max}^{1E}$	$\hat{\theta}_{\max}^{1I\&2E}$		$\hat{\theta}_{\max}^{1E}$
	Full-frame	Fishbone	Fishbone	Full-frame	Fishbone	Fishbone
Far-field	1.15	1.28	1.69	0.15	0.18	0.43
Kobe	1.23	1.16	1.07	0.26	0.26	0.37
Pulse-like	1.31	1.23	1.40	0.20	0.16	0.55

far-field earthquake records, 0.02 to 0.05 rad for the Kobe set, and 0.02 to 0.12 rad (approximately a ductility of 12) for the pulse-like earthquake records. The values of a and σ obtained using these fishbone results versus those for the full-frame model are compared in Table III. For all three sets of earthquake records, the estimates of a obtained using the fishbone results are within 10% of those obtained using the full-frame results. Similarly, the estimates of σ are not (statistically) significantly different.

It is interesting to note from Figure 3 that the four regression fits (i.e., values of a and σ) are roughly the same despite the different earthquake record sets and ranges of $\theta_{\max}$ values. As discussed in Reference [8], such results point to the 'sufficiency' of $\hat{\theta}_{\max}^{1I\&2E}$—that is, that the bias (and perhaps precision) of the predictor $\hat{\theta}_{\max}^{1I\&2E}$ does not significantly depend on the type of earthquake records considered. In Section 9.3 to follow (specifically Figure 5), we do not find this to be the case for $\hat{\theta}_{\max}^{1E}$.

8.3. JP4 and SAC20 buildings and nearby-field earthquake records

The bias and precision of $\hat{\theta}_{\max}^{1I\&2E}$ based on the fishbone model results for the JP4 and SAC20 buildings subjected to the nearby-field earthquake records are as follows: $a = 1.04$ and $\sigma = 0.17$ for JP4, and $a = 1.64$ and $\sigma = 0.32$ for SAC20. The corresponding estimates of a and σ using the full-frame models are about the same: $a = 1.09$ and $\sigma = 0.15$ for JP4, and $a = 1.58$ and $\sigma = 0.29$ for SAC20. It is important to note here that a and σ are smaller for JP4 than for SAC20. In fact, compared to the results for both JP4 and SAC9, $\hat{\theta}_{\max}^{1I\&2E}$ significantly underpredicts $\theta_{\max}$ for the SAC20 model, particularly in the elastic range (i.e., $\theta_{\max}$ less than about 0.01 rad). Additional (unpublished) results have shown that by also accounting for the third mode of (elastic) response, the predictions in the elastic range can be significantly improved without altering much the results in the inelastic range. In general, though, the bias and precision of a predictor can be significantly different for different buildings.

8.4. Summary

In summary, evaluating the bias and precision of predictors using fishbone models is demonstrated to be about the same as using the corresponding full-frame models, which are significantly

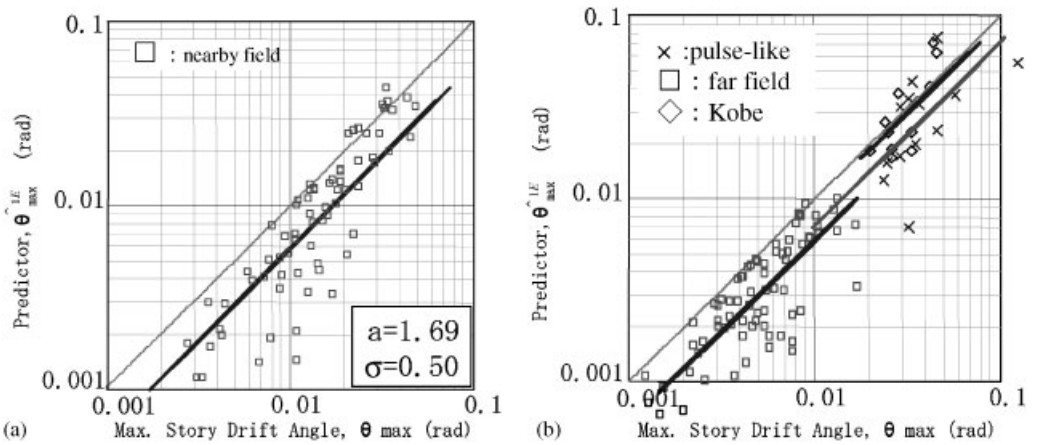

Figure 5. Regressions of $\theta_{\max}$ on $\hat{\theta}^{1E}_{\max}$ for the fishbone model of the SAC9 building subjected to (a) the nearby-field, and (b) the far-field, Kobe, and pulse-like sets of earthquake records. For the latter, the regression estimates of the bias (a) and precision (σ) of the predictor are listed in Table III.

more time-consuming to analyze. This is confirmed for all three of the buildings considered, as well as for the four different sets of ground motions. Given the strong correlation between fishbone and full-frame results found in References [5, 6], this result is not unexpected.

9. COMPARISON OF BIAS AND PRECISION OF PREDICTORS

Having demonstrated the equivalency of using fishbone versus full-frame buildings models in evaluating a predictor, here we will quantify the bias and precision of $\hat{\theta}^{1I\&2E}$ relative to $\hat{\theta}^{1E}$ using fishbone results only. Recall that NDA of a fishbone model is much less time-consuming than analysis of a full-frame model—for the SAC20 building, for example, the difference is about a factor of 60. Results for the same combinations of buildings, earthquake records, and drift demands that were considered in the previous section are reported here. In addition, $\hat{\theta}^{1I\&2E}_{\max}$ and $\hat{\theta}^{1E}_{\max}$ are evaluated for the artificial short-period SAC9S fishbone model subjected to the nearby-field earthquake records. Like in the previous section for comparing the fishbone versus full-frame results, here the statistical significance of differences in the bias (a) and precision (σ) of $\hat{\theta}^{1I\&2E}$ versus $\hat{\theta}^{1E}$ are formally tested, but not reported in detail.

9.1. SAC9 building and nearby-field earthquake records

To be compared with Figure 3(a), the regression of (i) the $\theta_{\max}$ values from NDA of the SAC9 fishbone model subjected to the nearby-field earthquake records on (ii) the corresponding values of the predictor $\hat{\theta}^{1E}_{\max}$, is illustrated in Figure 5(a). Note that the dispersion about the regression fit (i.e., $\sigma = 0.50$) is more than two times larger than that found for the predictor $\hat{\theta}^{1I\&2E}_{\max}$ (i.e., $\sigma = 0.23$ from Figure 3(a)). In other words, in this case $\hat{\theta}^{1I\&2E}_{\max}$ is a much more precise predictor of $\theta_{\max}$ than is $\hat{\theta}^{1E}_{\max}$. The predictor $\hat{\theta}^{1I\&2E}_{\max}$ is also (statistically) significantly

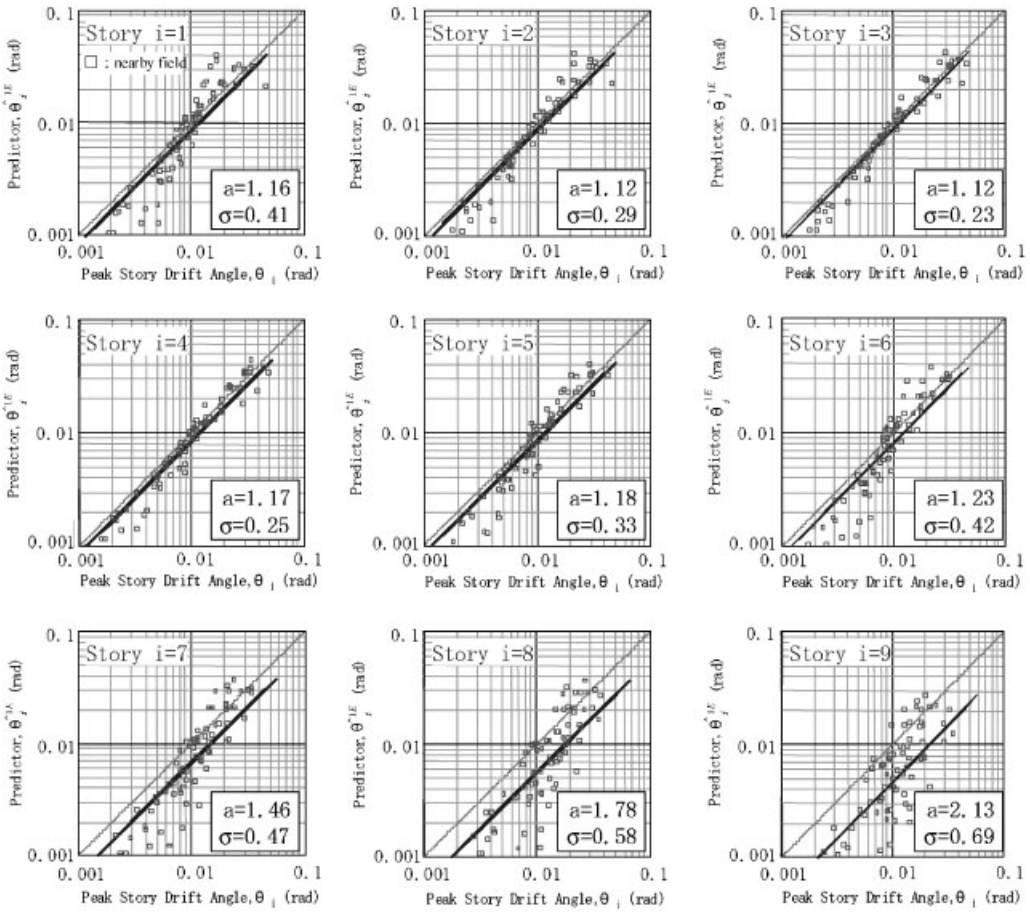

Figure 6. Regressions of θ_i on $\hat{\theta}_i^{1E}$ for the fishbone model of the SAC9 building subjected to the nearby-field earthquake records. Note the regression estimates of the bias (a) and precision (σ) of the predictor.

less biased than $\hat{\theta}_{\max}^{1E}$ ($a = 1.31$ vs. 1.69). It should be noted from Figure 5(a), though, that the bias of $\hat{\theta}_{\max}^{1E}$ is comparatively lower in the inelastic range than in the elastic range (i.e., $\theta_{\max}$ values less than about 0.01 rad); likewise, the dispersion about the regression fit is comparatively small in the inelastic range. As forewarned in Section 7, a number of the results presented in this paper show some evidence of a difference in the bias and/or precision of the predictor within the elastic versus inelastic ranges. These differences, however, are typically more pronounced for $\hat{\theta}_{\max}^{1E}$ than for $\hat{\theta}_{\max}^{1I\&2E}$ (e.g., Figure 5(a) compared to Figure 3(a)).

The analogous story-by-story regressions of θ_i on $\hat{\theta}_i^{1E}$ are illustrated in Figure 6, which is to be compared with Figure 4. The dispersions about the regression fits that employ $\hat{\theta}_i^{1E}$ as the predictor are significantly larger than those found using the predictor $\hat{\theta}_i^{1I\&2E}$, except in the 4th

story (where, even so, $\sigma = 0.25$ vs. 0.21). The predictor $\hat{\theta}_i^{1I\&2E}$ is especially precise relative to $\hat{\theta}_i^{1E}$ (by about a factor two) in the upper stories (i.e., 7th–9th), where the contribution of the second mode to the (elastic) response is most significant. Also in the upper stories, $\hat{\theta}_i^{1I\&2E}$ is significantly less biased than $\hat{\theta}_i^{1E}$, whereas in the other stories the biases of the two predictors are not significantly different.

9.2. SAC9 building and far-field, Kobe and pulse-like earthquake records

Still for the SAC9 fishbone model, but subjected to each of the other three suites of earthquake records, the regressions of $\theta_{\max}$ on the predictor $\hat{\theta}_{\max}^{1E}$ are illustrated in Figure 5(b). The resulting values of a and σ are listed in Table III, side-by-side with the results of regressing $\theta_{\max}$ on $\hat{\theta}_{\max}^{1I\&2E}$. For all three sets of earthquake records, $\hat{\theta}_{\max}^{1E}$ is less precise than $\hat{\theta}_{\max}^{1I\&2E}$, although the difference for the Kobe set ($\sigma = 0.37$ vs. 0.26) is not significant. The bias of $\hat{\theta}_{\max}^{1E}$ is also significantly larger than that of $\hat{\theta}_{\max}^{1I\&2E}$ for the far-field earthquake records (i.e., $a = 1.69$ vs. 1.13), but for the Kobe and pulse-like sets the differences in bias are not significant. As mentioned in Section 8.2, also note from Figure 5 that the regression fits for the four sets of earthquake records are somewhat different, suggesting that $\hat{\theta}_{\max}^{1E}$ is 'insufficient' [8].

9.3. JP4 and SAC20 buildings and nearby-field earthquake records

For the fishbone models of the JP4 and SAC20 buildings subjected to the nearby-field earthquake records, the results of regressing $\theta_{\max}$ on $\hat{\theta}_{\max}^{1E}$ are as follows: $a = 1.00$ and $\sigma = 0.25$ for JP4, and $a = 2.05$ and $\sigma = 0.56$ for SAC20. The corresponding results for $\hat{\theta}_{\max}^{1I\&2E}$ are summarized above in Section 8.3. As for SAC9, $\hat{\theta}_{\max}^{1E}$ is significantly less precise than $\hat{\theta}_{\max}^{1I\&2E}$ for both the JP4 and SAC20 fishbone models (i.e., $\sigma = 0.25$ vs. 0.17 and $\sigma = 0.56$ vs. 0.32, respectively). Both $\hat{\theta}_{\max}^{1E}$ and $\hat{\theta}_{\max}^{1I\&2E}$ are essentially unbiased for JP4 ($a = 1.00$ and 1.04), but $\hat{\theta}_{\max}^{1E}$ is significantly more biased than $\hat{\theta}_{\max}^{1I\&2E}$ for SAC20 ($a = 2.05$ vs. 1.64).

9.4. SAC9S fishbone model and nearby-field earthquake records

The results comparing $\hat{\theta}_{\max}^{1E}$ and $\hat{\theta}_{\max}^{1I\&2E}$ described above are consistent with those found in References [7, 8] for full-frame models of moderate- ($\sim$1 sec) to long- ($\sim$4 sec) period SMRF buildings. Here, in addition, we evaluate the predictors $\hat{\theta}_{\max}^{1E}$ and $\hat{\theta}_{\max}^{1I\&2E}$ for the short-period SAC9S fishbone model ($T_1 = 0.22$ sec). Recall that this entirely artificial model is obtained by simply increasing the stiffness (i.e., modulus of elasticity) of the fishbone model of the SAC9 by a factor of 100.

For the SAC9S fishbone model subjected to the nearby-field earthquake records, the regressions of $\theta_{\max}$ on $\hat{\theta}_{\max}^{1E}$ and on $\hat{\theta}_{\max}^{1I\&2E}$ are illustrated in Figure 7. It should be noted that the yield drift angle for SAC9S is about a factor of 100 less than the 0.01 rad estimated for SAC9. From Figure 7(a) it is evident that (i) the inelastic $\theta_{\max}$ response is substantially larger than that predicted by the elastic $\hat{\theta}_{\max}^{1E}$, even though the second-mode contribution to the elastic response is relatively small for this short-period structure, and (ii) the dispersion of $\theta_{\max}$ given $\hat{\theta}_{\max}^{1E}$ is also relatively large. Several researchers have observed both of these

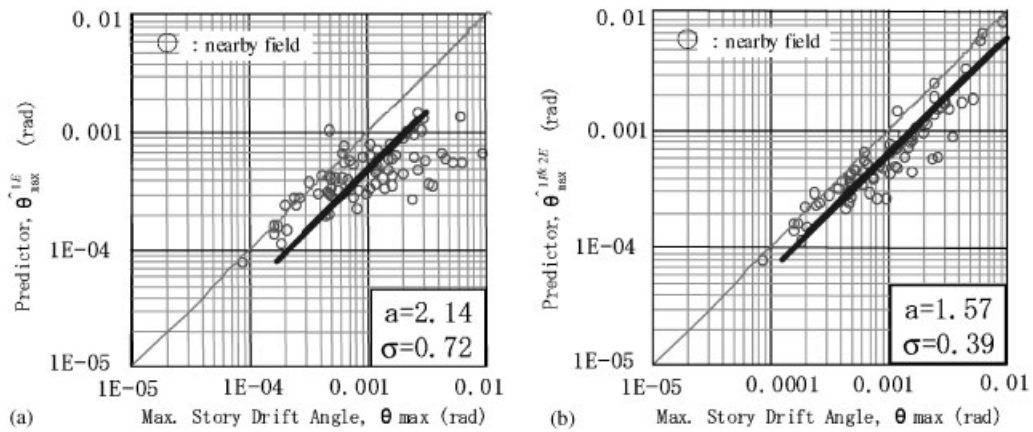

Figure 7. Regressions of $\theta_{\max}$ on (a) $\hat{\theta}^{1E}_{\max}$ and (b) $\hat{\theta}^{1I\&2E}_{\max}$ for the SAC9S fishbone model subjected to the nearby-field earthquake records. Note the regression estimates of the bias (a) and precision (σ) of the predictors.

phenomena for short-period SDOF systems, e.g., Reference [21]. By incorporating the inelastic spectral displacement, on the other hand, the predictor $\hat{\theta}^{1I\&2E}_{\max}$ is significantly less biased ($a = 1.57$ vs. 2.14) and more precise ($\sigma = 0.39$ vs. 0.72), as illustrated in Figure 7(b). Still, the precision of $\hat{\theta}^{1I\&2E}_{\max}$ for this short-period structure is less than that for the moderate- and long-period buildings considered. Note also that the bias of $\hat{\theta}^{1I\&2E}_{\max}$ for SAC9S is larger than that observed for the JP4 and SAC9 fishbone models, and about the same as that for the SAC20 fishbone model. Although not reported here in detail, both the bias and precision of $\hat{\theta}^{1I\&2E}_{\max}$ for SAC9S can be improved significantly by using (to compute the inelastic spectral displacement component of $\hat{\theta}^{1I\&2E}_{\max}$) a trilinear, rather than bilinear, backbone curve that more closely matches the non-linear static pushover curve. For the other, moderate- to long-period building models considered, however, a trilinear backbone curve does not significantly improve the bias or precision of $\hat{\theta}^{1I\&2E}_{\max}$.

9.5. Summary

In summary, the predictor $\hat{\theta}^{1I\&2E}_{\max}$ is demonstrated to be equally or less biased and relatively precise in comparison to the more conventional predictor $\hat{\theta}^{1E}_{\max}$. For the low-rise JP4 and (artificial) short-period SAC9S fishbone models this is mostly a consequence of the inelastic spectral displacement in $\hat{\theta}^{1I\&2E}_{\max}$, whereas for the long-period high-rise SAC20 building it is mostly the consideration of higher modes that improves the precision and bias of $\hat{\theta}^{1I\&2E}_{\max}$ over that of $\hat{\theta}^{1E}_{\max}$; for the mid-rise SAC9 building, both effects are influential. It should also be noted that while the values of the bias and precision of $\hat{\theta}^{1I\&2E}_{\max}$ for a given building model subjected to different types of earthquake records (e.g., far- versus nearby-field) are found to be roughly the same, the bias and precision of $\hat{\theta}^{1E}_{\max}$ can be significantly different for different types of buildings (e.g., SAC20 versus JP4).

10. CONCLUSIONS

An extension of the predictor $\hat{\theta}^{1E}$, which is proportional to first-mode-elastic spectral acceleration, the predictor $\hat{\theta}^{1I\&2E}$ takes into account the effects of inelasticity in addition to the elastic contributions of both the first and second modes. In this paper, $\hat{\theta}^{1I\&2E}$ is demonstrated to be equally or less biased, and equally or more precise, than $\hat{\theta}^{1E}$ in predicting linear and non-linear seismic drift demands for short- to long-period SMRF buildings subjected to near- and far-field ground motions. Furthermore, we demonstrate that the bias and precision of predictors can be evaluated using fishbone models of the buildings, with nearly the same results as those obtained using full-frame models, but with much less computational effort.

More specifically, for the moderate-period low-rise JP4 building ($T_1 = 0.75$ sec), $\hat{\theta}^{1I\&2E}_{\max}$ is essentially unbiased. For the longer-period mid-rise SAC9 building ($T_1 = 2.24$ sec), $\hat{\theta}^{1I\&2E}_{\max}$ is slightly biased low—that is, on average it under-predicts the value of $\theta_{\max}$ from NDA (non-linear dynamic analysis) by 10–25%. For the long-period high-rise SAC20 building ($T_1 = 3.82$ sec) and the artificial short-period SAC9S model ($T_1 = 0.22$ sec), however, $\hat{\theta}^{1I\&2E}_{\max}$ over-predicts the value of $\theta_{\max}$ from NDA by about 60% (i.e., it is biased high). Perhaps more important than the magnitude of the bias of $\hat{\theta}^{1I\&2E}_{\max}$ is its precision, because the bias of a precise predictor can be accurately estimated with relatively few NDAs (as discussed in Section 8.1). For all but the SAC9S model, $\hat{\theta}^{1I\&2E}_{\max}$ is relatively precise. Even up to large ductilities (of about 10) the dispersions of $\theta_{\max}$ given the value of the predictor are less than about 30% for SAC9 and SAC20 and less than 20% for JP4; for the SAC9S model, the dispersion approaches 40%, but if a trilinear backbone curve is used to compute $\hat{\theta}^{1I\&2E}_{\max}$, the dispersion is reduced to about 20%. Note that in Reference [7], $\hat{\theta}^{1I\&2E}$ is also found to be unbiased and relatively precise for predicting average (over all stories) peak story drift angles of a full-frame SAC9 model.

As demonstrated for the SAC9 building, the bias and precision of the story-specific predictor $\hat{\theta}^{1I\&2E}_i$ is not uniformly as good as $\hat{\theta}^{1I\&2E}_{\max}$, presumably due to more localized effects such as P–Δ and the isolation of upper stories because of yielding in lower stories, which can both be significant for mid- to high-rise, longer-period structures like SAC9 and SAC20. With the hope of improving its predictive power, a modification of $\hat{\theta}^{1I\&2E}$ that assumes a first-mode shape different than the elastic one, i.e., one based on story-drift results from a non-linear static pushover analysis, is a topic of ongoing research [22]. The 'modal pushover analysis' procedure recently proposed by Chopra and Goel [23], which is somewhat similar in concept to $\hat{\theta}^{1I\&2E}$ but more involved, uses (to estimate θ) story-drift results from non-linear static pushover analyses in addition to the elastic mode shapes. These types of potential improvements, however, make the predictor more complex and therefore may render it less useful, particularly for preliminary or conceptual design purposes. At some point, one might as well analyze the fishbone models themselves as predictors of seismic demands. Even in the first stages of design, a set of story strengths and stiffnesses for a fishbone frame can be roughly estimated for assumed (or design) earthquake forces, expected ductility (or strength-reduction factor), and expected story drifts.

Besides the four structures considered in this paper, additional structures of different fundamental periods, heights, and configurations should be used to further evaluate the predictor $\hat{\theta}^{1I\&2E}$. Fortunately, the computational efficiency of the fishbone model makes it possible to

consider many more buildings and earthquake ground motions. The use of fishbone models, however, is limited to buildings that are 'regular' in plan (but not necessarily in elevation), as explained in Reference [6]. It still remains to be shown whether $\hat{\theta}^{1I\&2E}$ is more biased and less precise for structures that are irregular in elevation and/or plan; at a minimum, $\hat{\theta}^{1I\&2E}$ is limited by the accuracy of non-linear static pushover analysis for such structures, as described in Reference [24] for example. Nonetheless, for the predominant class of regular buildings, the predictor $\hat{\theta}^{1I\&2E}$ can be useful in both structural performance assessment and design.

APPENDIX A: DETERMINING d_y AND α FROM A NSP CURVE

In calculating the predictor $\hat{\theta}^{1I\&2E}$, or more specifically the inelastic spectral displacement component $S_{\mathrm{d}}^{I}(T_1, \zeta_1, d_y, \alpha)$, we establish the yield displacement (d_y) and strain-hardening ratio (α) from a base-shear versus roof-drift-angle NSP (non-linear static pushover) curve for the building model. Since d_y and α are properties of an SDOF oscillator that is meant to represent the first mode of the building model, a 'first-mode' lateral load pattern is applied during the NSP analysis. Derived from modal analysis [9], the first-mode lateral load applied at the i-th floor of a building model, denoted F_i, is given by Equation (A1), where m_i, $\phi_{1,i}$, and n are defined in Section 3.1, and V_{b} is the total base shear. Note that the simple lateral load patterns specified in building codes [25] typically approximate the first-mode pattern.

$$F_i = \frac{m_i \phi_{1,i}}{\sum_{k=1:n} m_k \phi_{1,k}} V_{\mathrm{b}} \tag{A1}$$

The resulting first-mode NSP curves for the JP4, SAC9, and SAC20 building models (fishbone and full-frame models) were shown in Figure 2. In each of these cases, we used an elastic–perfectly-plastic (i.e., $\alpha = 0\%$) idealization of the NSP curve to determine d_y, because the curves are either nearly plastic or degrading. The elastic slope of the idealization follows the elastic points of the NSP curve, whereas the perfectly-plastic slope passes through the peak base shear (up to a roof drift angle of 0.10 rad). The intersection of the two slopes provides an estimate of the roof drift angle at yield, denoted $(\theta_{\mathrm{roof}})_y$, which is translated to d_y according to Equation (A2).

$$d_y = \frac{(\theta_{\mathrm{roof}})_y}{PF_1^{\theta_{\mathrm{roof}}}} \quad \text{where} \quad PF_1^{\theta_{\mathrm{roof}}} = \frac{\Gamma_1 \phi_{1,n}}{h_n} \tag{A2}$$

Recall that Γ_1, $\phi_{1,n}$, h_n, and n were defined in Section 3.1. The resulting values of d_y for the fishbone and full-frame models of the JP4, SAC9, and SAC20 buildings are listed in Table I.

For the SAC9S fishbone model, the first-mode NSP curve is shown in Figure A1. Unlike the NSP curves for the other three building models, note the significant post-elastic stiffness. The effects of P–Δ for SAC9S are insignificant relative to the large stiffness of the structure, even in the inelastic range. To reflect this difference, a bilinear rather than an elastic–perfectly-plastic backbone is fit to the NSP curve. In this case, the second slope is set to pass through the NSP curve at roof drift angles of 0.02 rad (assumed to correspond to a ductility of about 2) and 0.10 rad (beyond which the validity of the model is suspect). Otherwise, the procedure for determining d_y is the same as that described above for the elastic–perfectly-plastic case. The resulting estimates of d_y and α for SAC9S are listed in Table I; note that $\alpha = 3\%$ is

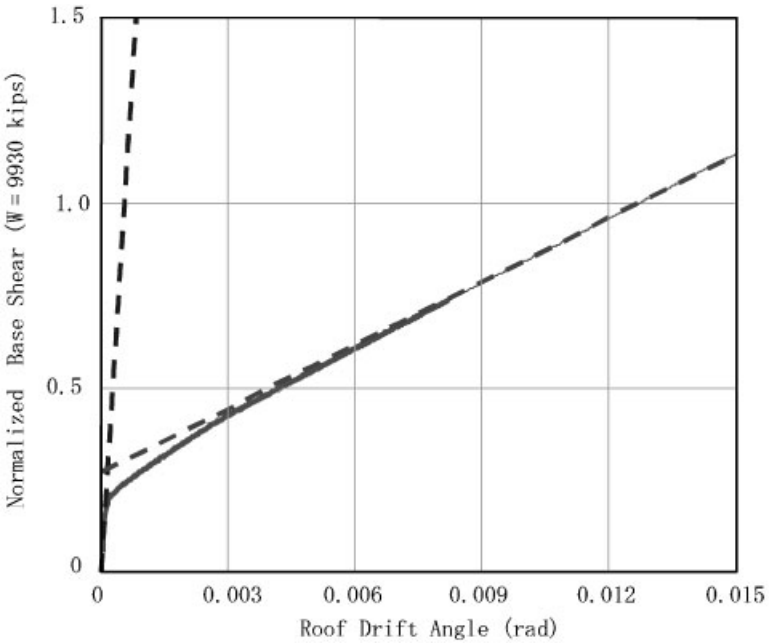

Figure A1. Non-linear static pushover curve for the SAC9S fishbone model, and the bilinear backbone curve fit to it.

equal to the strain hardening used for the beam and column elements. As mentioned in Section 9.4, a trilinear idealization of the NSP curve (with an additional intermediate slope) further improves the precision and bias of $\hat{\theta}_{\max}^{1I\&2E}$ for SAC9S. Particularly for non-SMRF buildings, a more sophisticated bilinear idealization (e.g., equal area under the NSP curve and its fit) could also prove to be more appropriate.

ACKNOWLEDGEMENTS

The authors gratefully acknowledge the financial support of the U.S.–Japan Cooperative Research in Urban Earthquake Disaster Mitigation Project (NSF 98-36) under grant number CMS-9821096, and the Grant-in-Aid for Scientific Research (B) (No.11209204) from the Ministry of Education, Science, Sports, and Culture and Japan Society for the Promotion of Science. The writers are also grateful to Dr T. Iwata of Kyoto University for his valuable instructions and comments on the near-fault ground motion records obtained from the Kobe earthquake.

REFERENCES

1. Collins KR, Wen YK, Foutch DA. Dual-level seismic design: a reliability-based methodology. *Earthquake Engineering and Structural Dynamics* 1996; **25**:1433–1467.
2. FEMA 351. Recommended seismic evaluation and upgrade criteria for existing welded steel moment-frame buildings. *SAC Joint Venture*; Sacramento, California, 2000.

3. Cornell CA. Calculating building seismic performance reliability: a basis for multi-level design norms. *Proceedings of the 11th World Conference on Earthquake Engineering*, Mexico, 1996; No. 2122.
4. Cornell CA, Jalayer F, Hamburger RO, Foutch DA. The probabilistic basis for the 2000 SAC/FEMA steel moment frame guidelines. *Journal of Structural Engineering* (*ASCE*) 2002; **128**(4):526–533.
5. Ogawa K, Kamura H, Inoue K. Modeling of moment resisting frame to fishbone-shaped frame for response analysis. *Journal of Structural and Construction Engineering* (*AIJ*) 1999; **521**:119–126 (in Japanese).
6. Nakashima M, Ogawa K, Inoue K. Generic frame model for simulation of earthquake responses of steel moment frames. *Earthquake Engineering and Structural Dynamics* 2002; **31**(3):671–692.
7. Luco N. Probabilistic seismic demand analysis, SMRF connection fractures, and near-source effects. *Ph.D. Dissertation*, Department of Civil and Environmental Engineering, Stanford University, Stanford, California, 2002.
8. Luco N, Cornell CA. Structure-specific scalar intensity measures for near-source and ordinary earthquake ground motions. Under revision for publication in *Earthquake Spectra*, 2003.
9. Chopra AK. *Dynamic of Structures*: *Theory and Applications to Earthquake Engineering*; 1st Edition. Prentice Hall: New Jersey, 1995.
10. Veletsos AS, Newmark NM. Effect of inelastic behavior on the response of simple systems to earthquake motions. *Proceedings of the 2nd World Conference on Earthquake Engineering*, Tokyo, Japan, 1960; 895–912.
11. Prakash V, Powell GH, Campbell S. DRAIN-2DX: Base program description and user guide, version 1.10. *Report No. UCB/SEMM-93/17*; Department of Civil Engineering, University of California at Berkeley, Berkeley, California, 1993.
12. FEMA 355C. State of the art report on systems performance of steel moment frames subject to earthquake ground shaking. *SAC Joint Venture*; Sacramento, California, 2000.
13. The Building Research Institute and Kozai Club. Evaluation of plastic deformation responses of steel moment frames subjected to earthquake motions. *Report of Committee on Numerical Analysis Procedures* 1995.
14. Liu J, Astaneh-Asl A. Cyclic testing of simple connections including effects of slab. *Journal of Structural Engineering* (*ASCE*) 2000; **126**(1):32–39.
15. Nakashima M, Matsumiya T, Asano K. Comparison in earthquake responses of steel moment frames subjected to near-fault strong motions recorded in Japan, Taiwan, and the U.S. *International Workshop on Annual Commemoration of Chi-Chi Earthquake*, Taipei, Taiwan, 2000; 112–123.
16. Alavi B, Krawinkler H. Effects of near-fault ground motions on frame structures. *John A Blume Earthquake Engineering Center Report No. 138*; Department of Civil and Environmental Engineering, Stanford University, Stanford, California, 2000.
17. Somerville PG, Smith N, Punyamurthula S, Sun J. Development of ground motion time histories for phase 2 of the FEMA/SAC steel project. *Report No. SAC/BD-97/04*; SAC Joint Venture, Sacramento, California, 1997.
18. Somerville PG. Development of an improved ground motion representation for near fault ground motions. *SMIP98 Seminar on Utilization of Strong-Motion Data*; Oakland, California, 1998.
19. Goel RK, Chopra AK. Period formulas for moment-resisting frame buildings. *Journal of Structural Engineering* (*ASCE*) 1997; **123**(11):1454–1461.
20. Rice JA. *Mathematical Statistics and Data Analysis*, 2nd Edition. Duxbury Press: California, 1995.
21. Sakamoto J, Kohama Y, Mori Y. A statistical representation of earthquake load effects for use in reliability-based design. *Proceedings of ICOSSAR '85, the 4th International Conference on Structural Safety and Reliability*, Kobe, Japan, 1985; II/217–II/226.
22. Funahashi Y, Mori Y, Nakashima M. Estimation of maximum displacement response of multi-story frame considering modal shape after yielding. *Summaries of Technical Papers of Annual Meeting*, *AIJ* 2002; **9**:57–58 (in Japanese).
23. Chopra AK, Goel RK. A modal pushover analysis procedure for estimating seismic demands for buildings. *Earthquake Engineering and Structural Dynamics* 2002; **31**(3):561–582.
24. Krawinkler H, Seneviratna GDPK. Pros and cons of a pushover analysis of seismic performance evaluation. *Engineering Structures* 1998; **20**:452–464.
25. FEMA 273. NEHRP guidelines for the seismic rehabilitation of buildings. *Federal Emergency Management Agency*; Washington, D.C., 1997.

